Toward Benchmarking Locomotion Economy Across Design Configurations on the Modular Robot: AMBER3M

Eric Ambrose[1], Wen-loong Ma[1], Christian Hubicki[1] and Aaron D. Ames[2]

Abstract— Making conclusive performance comparisons of bipedal locomotion behaviors can be difficult when comparing across different robots. This is particularly true in the case of comparing energy economy, which is highly dependent on mechanical, electrical and control components. As a means of controlling for these disparities for methodical testing, we designed and built a bipedal robot platform with modular legs, AMBER 3M. Three leg configurations were designed for this purpose: actuated flat feet, passive rigid point-feet, and compliant point-feet. As a proof of concept for the design's mechanical, electrical, and algorithmic modularity, we present walking experiments with all three AMBER 3M configurations, using the same control methods and experimental procedures. As a pilot study for investigating locomotion economy, we further performed systematic experiments with point foot walking with the purpose of examining the effects of speed on the cost of transport (COT); a long-studied trade-off in animals and simulations, but not in robotic hardware. We optimized a set of 36 walking gaits for maximum locomotion economy with various transport velocities. Walking performance data was collected from these gaits spanning a speed range of $0.34 \, \mathrm{m/s}$ to $0.94 \, \mathrm{m/s}$. An apparent Pareto-optimal frontier was observed in the data, showing that mechanical cost of transport increases with speed; ranging from 0.22 up to 0.36. Conversely, the electrical cost of transport remained approximately constant across observed walking speeds.
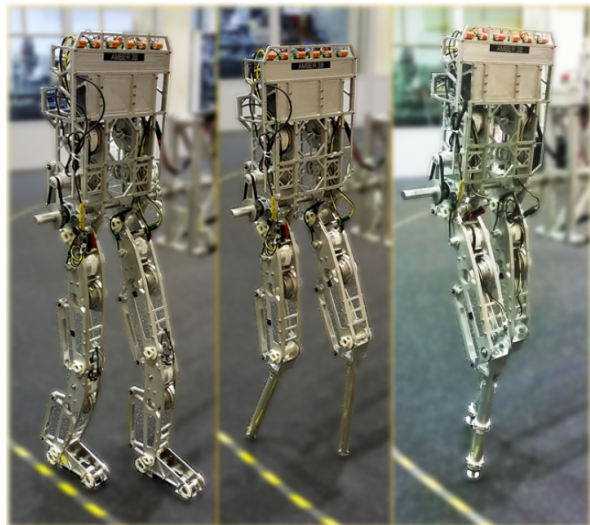
Fig. 1: AMBER 3M: Modular Bipedal Robot. A robot designed to test locomotion economy across three configurations: Flat-Foot (left), Point-Foot (center), Spring-Foot (right).

I. INTRODUCTION

In the field of bipedal locomotion, significant importance has been placed on optimizing a robot's motion for improved locomotion economy [6]. It is common to modify control methods and joint trajectories as means of lowering the cost of transport. However, even the most effective control schemes will still be subject to the natural dynamics involved with the robot's design. Therefore, the mechanical design of the robot should also be optimized for the desired behavior. This still presents an issue with making comparisons across different behaviors; for example: comparing flat-foot walking to point-contact walking. Once a robot has been optimally designed for one behavior, it is not necessarily the best option for another. In some cases, a robot can be specialized to the point of performing a single stable motion. In this paper, we demonstrate the use of a single robot performing multiple

behaviors in a way which allows for reasonable comparisons of locomotion economy.

Just as robots can be optimized for a task, animals seem to have the inherent ability to optimize their motion as well. Animals have been observed performing certain behaviors at speeds that are optimal for energy cost, [24]. The versatile anatomy of animals permits them to find ways of performing a remarkable number of behaviors. This range of ability has allowed research comparing the effectiveness of multiple behaviors for a given task. This was seen in [7], where the metabolic cost of transport of horses was measured during both trotting and galloping for the same speeds. This type of comparison would be useful for robots with options for performing a task [22]; for example, walking with either a flat-foot or a multi-contact "heel-to-toe" behavior.

Some labs have taken the first steps towards using a single robot for multiple behaviors. In some cases, simulation of both behaviors were developed for comparisons. In [21], walking and running were both investigated for optimal energy cost using mechanics-based models. Other groups have taken robots that have already been tested in experiment and run simulation of new behaviors. The authors of [12] did a simulation analysis of 3D running for the DURUS

[1]E. Ambrose, Wen-loong Ma, and Christian Hubicki are with the Department of Mechanical Engineering, Georgia Institute of Technology, Atlanta, USA. `{eambrose, wenlongma, christian.hubicki}@gatech.edu`

[2]Prof. A. Ames is with the Departments of Mechanical Engineering and Electrical Engineering, Georgia Institute of Technology, Atlanta, USA. `ames@gatech.edu`

robot, which had been previously shown to be a thoroughly efficient walker in experiments [18]. Beyond DURUS, there have been a numerous robots performing various locomotion behaviors across a range of efficiency [5], speed [20], and even rough terrain [14]. Since these robots have numerous practical differences, it can be difficult to identify what is responsible for their performance: their design, control, or both?

There have been instances of individual robots being used to reasonably compare multiple control methods for a given behavior, as in [27]. This type of comparison works well because only the controller is changed, while every other part of the robot and experiment is constant. Similar methods have been used but for the design's effect on energy economy[15], [19], [17]. However, comparisons between different behaviors (i.e. flat-foot walking and point-foot walking) tend to involve comparing two different robots, each performing one of the tasks. Being able to keep testing procedures, control hardware, and power systems constant between robots would allow for more controlled comparisons. A simple way to ensure this is to use a single robot, capable of performing all of the tasks with minimal changes made to the hardware. This was the motivation for the robot, AMBER3M.

This paper is constructed as follows. Section II covers the design and hardware capabilities of the modular robot AMBER 3M. Section III describes the methods of controlling and creating gaits for the robot. Section IV relays the procedures and experiments for testing walking with three different leg configurations along with an in depth investigation of a single behavior, point-foot walking. Lastly, Section V presents the result of each experiment along with some discussion.

II. DESIGN

With the aim testing a variety of bipedal robot design concepts, a new robot platform was developed: AMBER 3M. The purpose of this robot is to make switching between different behaviors and controllers much simpler, while still working with the same base system. The following section details the design of that base system and the method of switching between different behavior capabilities.

A. Mechanical Design of AMBER3M

AMBER 3M, seen in Fig. 1, is a planar bipedal robot designed and built at the Georgia Institute of Technology. The standard configuration of this robot stands 1.4 m tall, weighs 29.3 kg, and includes six actuated degrees of freedom. Each of these actuated joints is articulated via identical drive systems. The drive motors are capable of inputting 355 W of power, 2.2 Nm peak torque, and 0.66 Nm of continuous torque. The max motor speed is rated at 785 rad/s. The output of the motors is connected to a Harmonic gearhead (CSG-20-80-2UH-LW) through a timing belt with a 7:8 speed reduction. The Harmonic gearhead has a 1:80 gear reduction and roughly a 65% mechanical efficiency. The full system, including efficiency losses, is capable of a peak
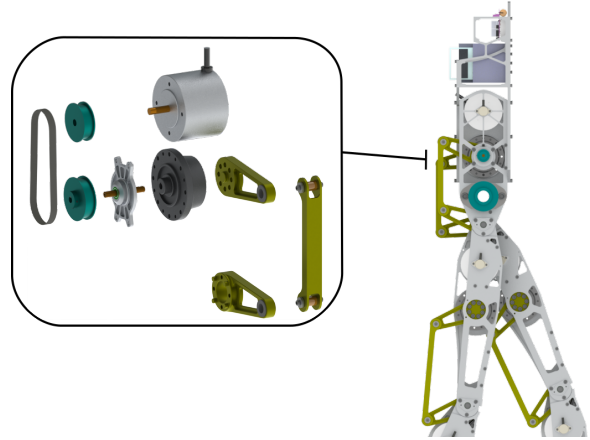

Fig. 2: An exploded view of the drive system for each joint of AMBER3M.

torque of 130 Nm, continuous torque of 39.2 Nm, and a max speed of 8.6 rad/s. The output of the gearhead is connected to the joint by linkages in a four-bar mechanism designed for a 1:1 input to output position ratio. The presence of linkages allows for the leg segments to be any length, without needing to change the drive system. An exploded view of these components is shown in Fig. 2. Rotor position and velocity feedback is provided by incremental encoders (Renishaw RM22IC) mounted to the back of each motor.

Since AMBER3M is a planar robot, a support structure is used to constrain it to the sagittal plane. This is accomplished through a circular boom which allows the robot to walk on an unending circular track, while still being fixed in the plane. The boom arm is 3.429 m long and arranged in a four-bar linkage. This linkage method allows for the arm to raise up and down without changing the angle of the end effector. The distal end of the boom connects to the robot via a rod passing through bearing mounts in the torso. The boom and robot connection can be seen in Fig. 1. The robot's torso is able to move in all three sagittal plane directions. The forward progression of the boom arm and the relative angle at the torso-boom connection are both measured by encoders, providing state information to the robot during experiments. Weights are placed on the end of the boom arm, opposite the robot, to counteract the weight of the arm itself. This counterbalancing is calibrated by balancing the arm when the robot is disconnected.

The torso of AMBER 3M acts as the control center of the robot. It houses the hip drives and all of the control electronics, and also distributes the power throughout the robot. A National Instruments (NI) cRIO-9033, running LabVIEW2015, is used as the high-level controller for the robot, reading in all of the state information from the joint encoders. Two world orientation encoders (torso-boom and boom rotation) are used to provide further state feedback and are connected to additional sensor modules mounted in the provided slots of the cRIO. The low-level control is provided
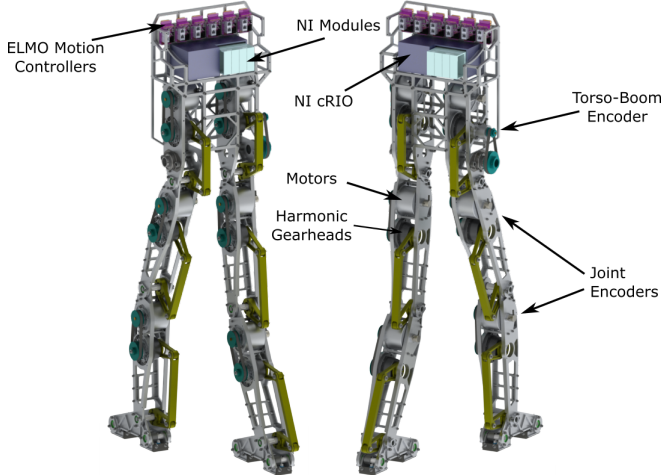
Fig. 3: Model indicating the placement of the key drive and control components within AMBER3M.

Fig. 4: Model views of the leg configurations tested on AMBER3M in the presented experiments: Flat Foot (left), Point Foot (center), Compliant Point Foot (Right).

by the motion controllers (ELMO G-SOL-WHI) controlling each motor via the joint encoders. Fig. 3 shows the placement of the control and drive components within AMBER3M.

B. Modularity

The key design feature of AMBER3M is the modularity of the legs. Each of the leg segments, from thigh to feet, are able to be removed from the rest of the robot individually. Furthermore, all joints on the robot have the same shape and functionality, with only two shafts holding a module to the one above it. The drive system for each joint is located within the segment above and connected through a stiff linkage. The encoder and motor power wires running down the legs can also disconnect individually, allowing for easy electrical connection as well. This simple connection style allows for portions of the leg to be swapped out in a matter of minutes. For the experiments described later in this paper, three different leg configurations were used. A CAD model view of each is provided in Fig. 4 and the general configuration properties are shown in Table I.

Flat-Foot Walking. In this standard leg configuration, AMBER3M has fully actuated ankle joints with feet. These feet can be used to walk with a multi-contact behavior, as in [26], but are only used for flat-foot walking in the experiment of this paper. The ankles use the same drive system described previously, and have pivoting toe and heel sections which allow them to conform to the ground.

Point-Foot Walking. As an alternative to the first case, a pair of rigid calves can be placed on the robot for when underactuated behaviors are desired. These calves do not have ankles or feet attached, but instead have a small rounded surface on bottom. This allows for a single point of contact and easy rotation between the legs and ground. It should be noted that the center of mass is above the hip for this configuration.

Compliant Point-Foot Walking. While these legs have a similar configuration to the previously described point-foot behavior, these calves now include a passive compression spring between the ground and knee. The springs have a stiffness of $17\,000\,\mathrm{N/m}$, and can deflect up to $3.5\,\mathrm{cm}$. There are linear variable differential transformer (LVDT) sensors placed within each calf to measure the spring deflection for potential use for state feedback (which is not utilized for the experiments presented). For ease of viewing these inner components of the calf in Fig. 4, the outer shell of the left leg has been removed.

III. CONTROL METHODOLOGY

This section defines the control, model, and optimization methods used to control AMBER-3M across three mechanical configurations. In an effort to explore the properties of energy-optimal gaits, we sought to implement a hardware-tested surrogate for optimal control. As a framework for control optimization, we used a hybrid zero dynamics (HZD) [23] implementation on which we optimized control for maximum locomotion economy [18]. HZD was selected for its generalizability to both fully- and under-actuated systems, and its track-record of successful hardware implementations.

A. Control

From the view of hybrid zero dynamics, control is the successful satisfaction of a set of *output* equations, in real time, on the robot via motion of its actuators. Importantly, these outputs are designed to be *impact invariant*, i.e., they must satisfy an HZD condition. As such, we will focus on presenting these output equations in a fashion which generalizes to all three AMBER3M hardware configurations. The difference in output equations across configurations manifest, inherently, from the construction of their respective

TABLE I: A list of the robot properties for each configuration.

Configuration	Weight	Height	CoM (from hip)
Flat-foot	29.3 kg	1.400 m	−0.161 m
Point-foot	21.9 kg	1.373 m	0.025 m
Spring-foot	23.5 kg	1.430 m	−0.024 m
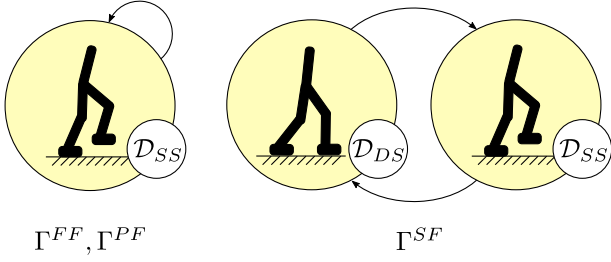
Fig. 5: Illustration of the flow of domains for the three design configurations.

Fig. 6: Depiction of the generalized coordinates for the three AMBER3B configurations.

underlying hybrid systems.

Hybrid Control System. The configuration-modular multi-domain hybrid control system is defined as a tuple [4], [25],

$$\mathcal{HC} = (\Gamma^i, \mathcal{D}^i, \mathcal{U}^i, S^i, \Delta^i, FG^i) \qquad (1)$$

where $\Gamma^i = (V^i, E^i)$ is a directed cycle and $i \in \{FF, PF, SF\}$ denotes the design configuration (flat, point, and spring feet respectively). $v^i \in V^i$ are vertices indicating domains of admissibility where $v^{FF} = v^{PF} = \{SS\}$ and $v^{SF} = \{SS, DS\}$ where SS and DS and single- and double-support phases of locomotion (spring legs have nontrivial durations with both feet in ground contact). Vertices are connected by edges, $e^i \in E^i$, where $e^i = \{v^i \to v^{i+}\}$, see Fig. 5.

For the hybrid control system $\mathcal{D}^i = \{\mathcal{D}^i_{v^i}\}_{v^i \in V^i}$ as the set of admissible domains of the system from a given configuration, given in (local) coordinates as $(q^i, \dot{q}^i, u^i) \in D^i_{v^i}$, where $q^i, \dot{q}^i$, and $u^i_{v^i}$ are coordinates positions, velocities and control inputs respectively. The control inputs for each configuration, $\mathcal{U}^i = \{\mathcal{U}^i_{v^i}\}_{v^i \in V^i}$ is the set of admissible controls with n^i_u control inputs where $\mathcal{U}^i_{v^i} \subseteq \mathbb{R}^{n^i_u}$; that is, admissible inputs $u^i_{v^i} \in \mathcal{U}^i_{v^i}$. We further define, $FG = \{FG^i_{v^i}\}_{v^i \in V^i}$, as the set of control systems on the admissible domains $\mathcal{D}^i_{v^i}$. On the edges, we define switching surfaces, $S^i = \{S^i_{e^i}\}_{e^i \in E^i}$, where $S^i_{e^i} \subset \mathcal{D}^i_{v^i}$ and reset maps, $\Delta^i = \{\Delta^i_{e^i}\}_{e^i \in E^i}$, that smoothly map between the source and domain of edges $e^i \in E^i$, i.e., $\Delta^i_{e^i} : \mathcal{D}^i_{v^i} \to \mathcal{D}^i_{v^{i+}}$. The predefined flow of these domains is illustrated in Fig. 5.

We now specialize to the robots under consideration, in which case the generalized coordinates, q^i, which differ across configurations, $q^i \in \mathcal{Q}^i_v \subset \mathbb{R}^{n^i}$ where $n^{FF} = 6$, $n^{PF} = 4$, and $n^{SF} = 4$. We further define the configuration/domain with specific local coordinates as follows: $q^{FF} = (q_{sa} \; q_{sk} \; q_{sh} \; q_{nsh} \; q_{nsk} \; q_{nsa})$, $q^{PF} = (q_{sf} \; q_{sk} \; q_{sh} \; q_{nsh} \; q_{nsk} \; q_{nsa})$, $q^{SF} = (q_{sf} \; q_{sr}; q_{sk} \; q_{sh} \; q_{nsh} \; q_{nsk} \; q_{nsr})$ as labeled in Fig. 6.

Continuous Dynamics. With this basic groundwork defined, we now define the continuous dynamics over our domains, $\mathcal{D}^i_{v^i}$. On these domains, the control systems $FG^i_{v^i}$ are obtained from the Euler-Lagrange equations [16]:

$$D(q^i)\ddot{q}^i + H(q^i, \dot{q}^i) = B_{v^i}u^i_{v^i} + (J^i_{v^i}(q^i))^T F^i_{v^i} \qquad (2)$$

subject to the holonomic constraints

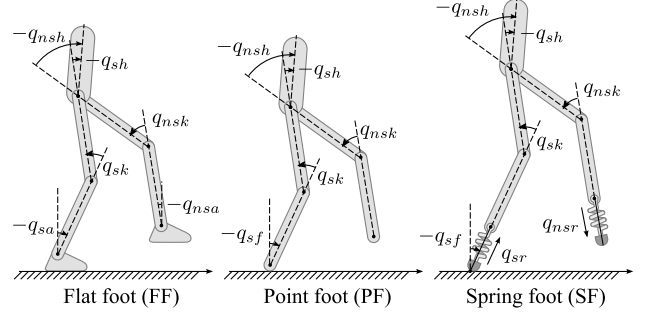$$J_{v^i}(q^i)\ddot{q}^i + \dot{J}_{v^i}(q^i, \dot{q}^i)\dot{q}^i = 0. \qquad (3)$$

Here, the contact wrenches, $F^i_{v^i}(q^i, \dot{q}^i, u^i_{v^i})$ [10], are different for each i, and thereby enforce the overall dynamics unique to each leg configuration (e.g., by correspondingly changing constraint forces corresponding to holonomic constraints). Manipulation of these equations of motion yields the control systems $FG^i_{v^i} = (f_{v^i}, g_{v^i})$ given by:

$$\dot{x}^i = f_{v^i}(x^i) + g_{v^i}(x^i)u^i_{v^i} \qquad (4)$$

where here $x^i = (q^i, \dot{q}^i)$ is the system state for a given robot configuration.

Outputs. With the goal of synthesizing controllers, and with the dynamics defined, we consider *outputs* or *virtual constraints* [9], [2] of the form:

$$y^i_{v^i}(q^i, \dot{q}^i) = \begin{bmatrix} y^i_{1,v^i}(q^i) \\ y^i_{2,v^i}(q^i, \dot{q}^i, \alpha^i_{v^i}) \end{bmatrix} \qquad (5)$$
$$= \begin{bmatrix} y^{a,i}_{1,v^i}(q^i) - y^{d,i}_{1,v^i} \\ y^{a,i}_{2,v^i}(q^i) - y^{d,i}_{2,v^i}(\tau(q^i), \alpha^i_v) \end{bmatrix}$$

where $y^{a,i}_{1,v} : Q^i \to \mathbb{R}$ and $y^{a,i}_{2,v} : Q^i \to \mathbb{R}^{n^i_{o,v}}$ define the "actual" relative degree 1 and 2 outputs respectively (see [3] for justification), where $n^i_{o,v}$ indicates the number of relative degree 2 outputs, with $n^{FF}_{o,SS} = 6$, $n^{PF}_{o,SS} = 4$, $n^{SF}_{o,SS} = 4$, and $n^{SF}_{o,DS} = 3$. For each domain, relative degree 2 outputs are defined for the flat-foot gait as $y^{d,FF}_{2,SS}(q^i) = [q_{sk}, q_{nsk}, \theta_{tor}(q^i), \delta m_{nsl}(q^i), q_{nsf}]^T$ where $\theta_{tor}(q^i)$ and $\delta m_{nsl}(q^i)$ are defined in [13]. The actual degree 2 outputs for the remaining domains are simple joint angles: $y^{d,PF}_{2,SS}(q^i) = [q_{sk}, q_{sh}, q_{nsh}, q_{nsk}]^T$, $y^{d,SF}_{2,SS}(q^i) = [q_{sk}, q_{nsk}, q_{sh}, q_{nsh}]^T$, and $y^{d,SF}_{2,DS}(q^i) = [q_{sk}, q_{sh}, q_{nsh}]^T$. For the relative-degree 1 outputs, $y^{a,FF}_{1,SS}(q^i)$ is the forward hip velocity [13] and $y^{a,PF}_{1,SS}(q^i) \equiv y^{a,SF}_{1,SS}(q^i) \equiv y^{a,SF}_{1,DS}(q^i) \equiv 0$.

Desired relative degree 2 outputs, $y^{d,i}_{2,v}(\tau(q^i), \alpha^i_v)$ are parameterized by Bézier polynomials [20]

$$y^{d,i}_{2,v}(\tau(q^i), \alpha^i_v) := \qquad (6)$$
$$\sum_{k=0}^{M} \alpha^i_v[k] \frac{M!}{k!(M-k)!} \tau(q^i)^k (1 - \tau(q^i))^{M-k}.$$

with $M+1$ coefficients contained in vector $\alpha_v^i \in \mathbb{R}^{M+1}$. These outputs are further parameterized by the phase variable $\tau(q^i)$, which increases with forward hip position, $\delta p_{hip}(q^i)$,

$$\tau(q^i) = \frac{\delta p_{hip}(q^i) - \delta p_{hip,v}^{i,+}}{\delta p_{hip,v}^{i,-} - \delta p_{hip,v}^{i,+}} \tag{7}$$

where $\delta p_{hip,v}^{i,+}$ and $\delta p_{hip,v}^{i,-}$ are the initial and final (expected) hip positions for a given domain.

Partial Hybrid Zero Dynamics. To drive these outputs to zero, we use feedback control. Our hybrid control system assumes a feedback linearizing control law [2],

$$u_{v^i}^\varepsilon(q^i, \dot{q}^i, \alpha_{v^i}^i) = -(\mathscr{A}_{v^i}^i)^{-1} \left(\begin{bmatrix} 0 \\ L_{f_{v,i}}^2 y_{2,v^i}^i(q^i, \dot{q}^i, \alpha_{v^i}^i,) \end{bmatrix} \right.$$
$$+ \left. \begin{bmatrix} L_{f_{v^i}} y_{1,v^i}^i(q^i, \dot{q}^i) \\ 2\varepsilon L_{f_{v^i}} y_{2,v^i}^i(q^i, \dot{q}^i, \alpha_{v^i}^i) \end{bmatrix} + \begin{bmatrix} \varepsilon y_{1,v^i}^i(q^i, \dot{q}^i) \\ \varepsilon^2 y_{2,v^i}^i(q^i, \alpha_{v^i}^i) \end{bmatrix} \right), \tag{8}$$

where $\mathscr{A}_{v^i}^i = [L_{g_{v^i}} y_{1,v^i}^i(q, \dot{q}) \quad L_{g_{v^i}} L_{f_{v^i}} y_{2,v^i}^i(q^i, \dot{q}^i, \alpha_{v^i}^i)]^T$ and $\varepsilon > 0$. This controller results in linear output dynamics $\dot{y}_{1,v^i}^i = -\varepsilon y_{1,v^i}^i$ and $\ddot{y}_{2,v^i}^i = -2\varepsilon \dot{y}_{2,v^i}^i - \varepsilon^2 y_{2,v^i}^i$. As a result of these output dynamics, the system is stable to the *partial zero dynamics surface* [1] given by:

$$\mathbf{PZ}_{v^i} = \{(q^i, \dot{q}^i) \in \mathscr{D}_{v^i}^i | y_{2,v^i}^i(q^i) = 0, \dot{y}_{2,v^i}^i(q^i, \dot{q}^i) = 0\}. \tag{9}$$

Further, for any $e^i \in E^i$, the submanifold $\mathbf{PZ}_{v^i}$, if there exists an $\{\alpha_{v^i}\}_{v \in V}$ so that

$$\Delta_{e^i}(x) \in \mathbf{PZ}_{v^i,+}, \qquad \forall x^i \in S_{e^i} \cap \mathbf{PZ}_{v^i}. \tag{10}$$

then the system is hybrid invariant and has *partial hybrid zero dynamics*. In such cases, the stability of the full order system reduces to the stability of the partial hybrid zero dynamics.

B. Efficient HZD Gait Optimization

To generate energy-efficient walking gait for the modular robot AMBER3M, this paper utilized a collocation based optimization algorithm integrated with the HZD based control scheme above. Our gait-optimization problem is defined by the following nonlinear program (NLP):

$$\mathbf{Z}^{i,*} = \underset{\mathbf{Z}}{\text{argmin}} \quad \sum_{v^i} \mathscr{J}_v(\mathbf{Z}_{v^i}^i) \tag{11}$$
$$\text{s.t} \quad \mathbf{Z}_{\min} \leq \mathbf{Z}_{v^i}^i \leq \mathbf{Z}_{\max}, \tag{12}$$
$$\mathbf{C}_{\min} \leq \mathbf{C}(\mathbf{Z}_{v^i}^i) \leq \mathbf{C}_{\max}, \tag{13}$$

where, $\mathbf{Z}_{v^i}^i$ is a vector of decision variables for the NLP, $\mathscr{J}_v(\mathbf{Z}_v^i)$ is the mechanical cost of transport (14) as the objective of the optimization, $\mathbf{Z}_{min}$ and $\mathbf{Z}_{max}$ are the enforced limits of each optimization variable, and $\mathbf{C}(\mathbf{Z}_{v^i}^i)$ is a vector of constraint functions. In this modular optimization problem, the constraints are chosen to be the HZD invariance, foot clearance, torso moving range and ZMP constraints. In particular, to generate gaits with different forward velocity for later study, we also encoded the average velocity as a nonlinear equality constraint. Due to the complex nonlinearity of

the dynamics and constraints, we employed a *pseudospectral method* [8] to improve the computational efficiency and reliability of this gait generation process. Essentially, this approach numerically approximates the time solution of the locomotion dynamics by trigonometric or orthogonal polynomials at chosen collocation points. In this case, we use Lagrange interpolating polynomials at Legendre-Gauss-Lobatto (LGL) grids. The computation of analytical constraint Jacobians further improved the algorithm's reliability and performance. More details can be found in [11].

IV. EXPERIMENTAL EVALUATION

To validate the concept of modularity of robot design experimentally, this framework also requires modularity of each component of the control structure, including mechanical, electrical, and controller implementation. This section will introduce the electrical system of AMBER3M first, then an experimental control procedure for AMBER3M walking is detailed. The effectiveness of the modular components will be shown through tests of each behavior. Finally, we present an extensive study of point-foot walking, providing a more-thorough analysis of locomotion economy for this type of behavior.

A. Experiment Configuration

The control framework of AMBER3M is composed of three levels: the high level controller, the low level controller and the data logger. In the high level, the on-board cRIO running RTLinux serves as the master board, communicating with the low level controller in a real-time fashion. Experimental data is sent to a remote desktop, which acts as the data logger. In the low level, the motor drivers deliver the desired torque-driven motion to their corresponding BLDC motors. Other modes of experimental feedback, such as the rotary boom states, torso rotation and electrical power consumption, are collected by an embedded FPGA board.

B. Realizing Multiple Walking Behaviors.

For a chosen leg configuration, an optimized gait can be reliably produced by the aforementioned optimization method. To realize the corresponding bipedal walking on AMBER3M, a real time controller was programmed in C++ and compiled onto the on-board master computer. A detailed pseudocode is presented in Algorithm 1 to illustrate the experimental control method. Detailed terminology explanations for the algorithm can be found in [13]. It is very important to notice that, for all three design configurations, the control method was purely PD feedback control without any type of pre-defined feedforward controller involved. And due to the modularity of the control structure, switching the controller among design configurations can be accomplished without restructuring code. To demonstrate to efficacy of the modular control framework, sustainable bipedal walking was realized on AMBER3M with the flat-foot, point-foot and compliant-point-foot design configurations. For each case, gaits were generated and tested using Algorithm 1. The robot

Algorithm 1 Real Time Controller

Input: AMBER 3M design configuration: $i \in \{FF, PF, SF\}$;
Input: Control type;
Input: AMBER 3M model parameters;
Input: Domain/Step switching flag: $\tau_{max,v}^i$;
Input: Optimization Parameters: $\delta Phip_v^{i,+}, \delta Phip_v^{i,-}, \alpha_v^i, q^{i,+}$;
Input: PD controller gains: K_p^i, K_d^i
Input: System states (Left/Right): $(q_{LR}^i, \dot{q}_{LR}^i)^T$
Input: L/R stance; Encoder status; Drive status;
Output: Enable/Disable motor drives;
Output: Desired torque for each BLDC motor;
1: Enable motor drives;
2: **repeat**
3:    Wait till all motor drives are enabled
4: **until** (Drive-Status == Enable)
5: **while** (¬ Stop-RT) **do**
6:    **if** Control type == Initialization **then**
7:       $q_d = q^{i,+}; \dot{q}_d = \mathbf{0}$;
8:    **else**
9:       Map $(q, \dot{q})^T$ from Left/Right to Stance/nonStance;
10:      Calculate phase variable $\tau = \tau(q^i)$;
11:      **if** $i == FF$ **then**
12:        Calculate (ξ_1, ξ_2) based on τ;
13:      **end if**
14:      Calculate $\dot{\tau}$;
15:      Calculate $(y_d, \dot{y}_d)$;
16:      Calculate $(q_d, \dot{q}_d)$ using PHZD reconstruction;
17:    **end if**
18:    Apply PD controller:
       $u^i = K_p^i(q_a - q_d) + K_d^i(\dot{q}_a - \dot{q}_d)$;
19:    Map u^i from Stance/nonStance to Left/Right;
20:    **if** $\tau > \tau_{max,v}^i$ **then**
21:       Switch to next domain v or next stance status.
22:    **end if**
23:    Sending torque command to motor driver;
24:    Log data into remote desktop;
25: **end while**
26: Disable motor drives;
27: Report errors and stop the Real-Time VI;

---

was able to walk three laps (21.55 m each) on the boom with the tested gaits, at which point the gait was deemed successful. Tiles of a single step from each of these walking behaviors are shown in Fig. 7. And the phase portrait of each design configuration are provided with experimental and simulated data in Fig. 8, demonstrating that the periodic walking was achieved with the proposed method.

C. Point-Feet Locomotion Economy.

An in-depth assessment of the rigid point-foot configuration followed initial testing. The objective of this work was to discover the energetic optimal limit for the point-foot walking over a range of transportation speeds. 36 walking gaits were generated covering a speed range of 0.34 m/s to 0.94 m/s and tested on AMBER3M. Note that these speeds are the average forward velocity of the Center of Mass of AMBER 3M in simulation. Due to the underactuated dynamics and model uncertainty, experimental velocities are not guaranteed to align with simulation results. For instance, at very slows speeds (less than 0.3 m/s), the insufficient kinetic energy of the simulated walking behavior could be consumed by the unmodeled friction, resulting in an even slower speed.

For each experiment, AMBER3M walked three laps (21.55 m each) on the boom. The experimental data was recorded over each of the three-lap trials. Since the robot walks around a circular boom, energy cost was analyzed for every two steps, or one stride, to average the asymmetric left and right behaviors. The mechanical cost of transport *MCOT* for j^{th} stride over the weight and distance traveled is calculated as:

$$MCOT_j = \frac{1}{Mgd_j} \int_{t_j^-}^{t_j^+} | u |^T | \dot{q} | \, dt \qquad (14)$$

where M is the total mass of the robot, g is the gravitational constant, and d_j is the distance traveled of the center of mass calculated by the kinematic model. The torque u is estimated from the measured current going through the motor, and the angular velocity $\dot{q}$ is measured by the incremental encoder mounted on each joint. These measurements were then plotted against their corresponding average forward velocities in Fig. 9.

As shown in the plot, it can be seen that six gaits occupied the lowest region of the plot which have been highlighted in the figure. Using these six gaits, a Pareto frontier can be created to represent the locomotion economy extreme for point-feet walking on AMBER3M. A clear trend can be observed in these optimal gaits, showing that the mechanical energy required to walk increases with walking speed.

Further, the electrical power consumption of all the motor drivers was measured directly from the DC power supply. With this data, we calculated the electrical cost of transport *ECOT* for j^{th} stride by

$$ECOT_j = \frac{1}{Mgd_j} \int_{t_j^-}^{t_j^+} IE \, dt \qquad (15)$$

where $E = 48.3V$ is the DC voltage of the power supply, and I is the total current going through all motor drivers. The electrical cost of transport for the six optimal gaits is shown in Fig. 10. It should be noted that this power data does not include the logic power consumed by the sensors and on-board computers. It is assumed that the additional power costs are relatively constant, and would not effect any trends seen in the data. In comparison with Fig. 9, where higher velocity tends to require higher mechanical energy, electrical power does not show a noticeable change with velocity.

V. CONCLUSIONS

A modular robot design was presented as a means of comparing locomotion economy for multiple bipedal gait behaviors. To show the physical capability of AMBER 3M to viably walk with all its leg modules, three different walking behaviors were implemented experimentally, one for each leg configuration. These preliminary results demonstrated that a single robotic platform and control methodology can be successfully realize stable walking across multiple designs (both fully- and underactuated). We optimized 30 gaits were used to further study locomotion economy for point-foot walking
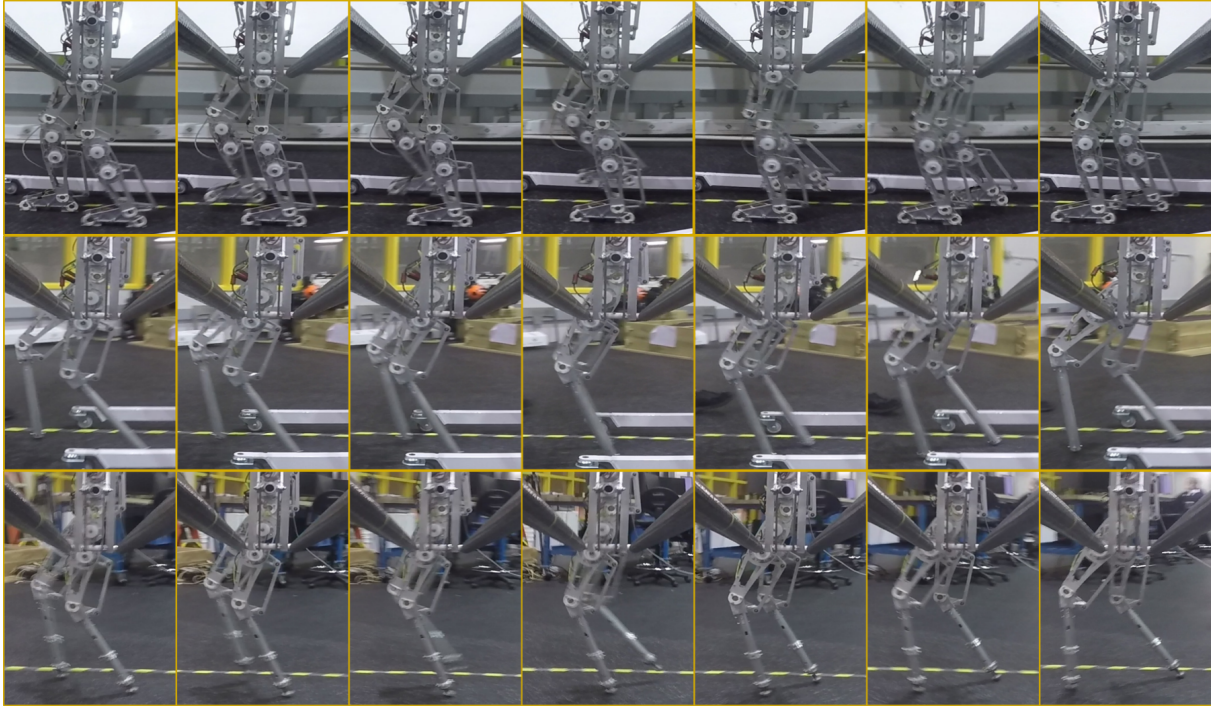
Fig. 7: Walking tiles for each of the three design configurations: Flat-foot (top), Point-Foot (middle), Compliant Point-Foot (bottom).

over a wide walking speed range. A Pareto-optimal frontier for locomotion economy was distilled, illustrating the peak observed energy performance of this design configuration at various speeds. Future work will focus on similar in-depth analysis for the flat-footed and spring-legged configurations, with the intent of further investigating the energetics of robotic bipedal locomotion.

VI. Acknowledgements

References

[1] A. D. Ames. Human-inspired control of bipedal robots. In *Conditionally accepted for publication in IEEE Transactions on Automatic Control*, 2012.

[2] A. D. Ames. Human-inspired control of bipedal robots via control lyapunov functions and quadratic programs. In *16th International conference on Hybrid systems: computation and control*, pages 31–32. ACM, 2013.

[3] A. D. Ames. Human-inspired control of bipedal walking robots. *Automatic Control, IEEE Transactions on*, 59(5):1115–1130, 2014.

[4] A. D. Ames, R. Vasudevan, and R. Bajcsy. Human-data based cost of bipedal robotic walking. In *Hybrid Systems: Computation and Control*, pages 153–162, Chicago, IL, 2011.

[5] P.A. Bhounsule, J. Cortell, A. Grewal, B. Hendriksen, J.G.D. Karssen, C. Paul, and A. Ruina. Low-bandwidth reflex-based control for lower power walking: 65 km on a single battery charge. *IJRR*, 33(10):1305–1321, Sep 2014.

[6] S. Collins, A. Ruina, R. Tedrake, and M. Wisse. Efficient bipedal robots based on passive-dynamic walkers. *Science*, 307:1082–1085, 2005.

[7] C.T. Farley and C.R. Taylor. A mechanical trigger for the trot-gallop tranisition in horses. *Science*, 253:306–308, 1991.

[8] D. Gottlieb and S. Orszag. *Numerical Analysis of Spectral Methods*. Society for Industrial and Applied Mathematics, 1977.

[9] J. W. Grizzle, C. Chevallereau, R. W. Sinnet, and A. D. Ames. Models, feedback control, and open problems of 3d bipedal robotic walking. *Automatica*, 50(8):1955 – 1988, 2014.

[10] A. Hereid, E. A. Cousineau, C. M. Hubicki, and A. D. Ames. 3D dynamic walking with underactuated humanoid robots: A direct collocation framework for optimizing hybrid zero dynamics. In *To appear in the IEEE International Conference on Robotics and Automation (ICRA)*. IEEE, 2016.

[11] A. Hereid, S. Kolathaya, and A. D. Ames. Online hybrid zero dynamics optimal gait generation using legendre pseudospectral optimization. In *to appear in IEEE Conference on Decision and Control*, 2016.

[12] W. Ma, A. Hereid, C.M. Hubicki, and A.D. Ames. Efficient hzd gait generation for three-dimensional underactuated humanoid running. 2016.

[13] W Ma, Huihua Zhao, Shishir Kolathaya, and Aaron D Ames. Human-inspired walking via unified pd and impedance control. In *submitted to the IEEE International Conference on Robotics and Automation*, 2014.

[14] I.R. Manchester, U. Mettin, F. Iida, and R. Tedrake. Stable dynamic walking over uneven terrain. *IJRR*, 30(3):265–279, Mar 2011.

[15] A.E. Martin, D.C. Post, , and J.P. Schmiedeler. The effects of foot geometric properties on the gait of planar bipeds walking under hzd-based control. *The International Journal of Robotics Research*, 33(12):1530–1543, 2014.

[16] R. M. Murray, Z. Li, and S. S. Sastry. *A Mathematical Introduction to Robotic Manipulation*. CRC Press, Boca Raton, March 1994.

[17] A. Ramezani, J. Hurst, K.A. Hamed, and J.W. Grizzle. Performance analysis and feedback control of atrias, a three-dimensional bipedal robot. *Journal of Dynamic Systems, Measurement, and Control*, 136, Dec 2013.

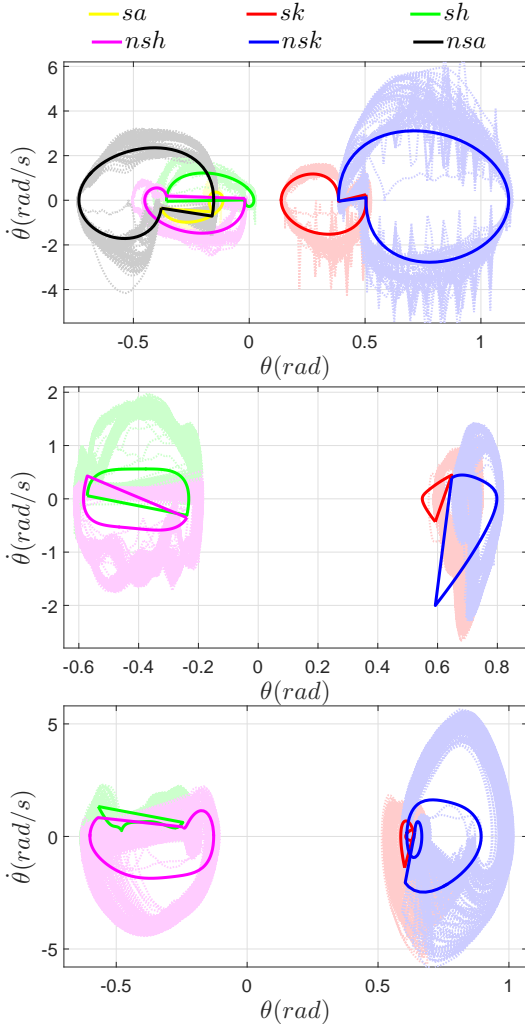[18] J. Reher, E.A. Cousineau, A. Hereid, C.M. Hubicki, and A.D. Ames.

Fig. 8: Phase portraits for each of the three behaviors: Flat-feet (top), Point-Feet (middle), Compliant-Point-Feet (Bottom).

Fig. 9: Plot of mechanical cost of transport vs walking speed for **(a)** all 36 successful gaits and **(b)** the six gaits on an apparent Pareto frontier of speed and energy economy.

Fig. 10: Plot of electrical cost of transport vs walking speed for the six optimal gaits

Realizing dynamic and efficient bipedal locomotion on the humanoid robot durus. In *Robotics and Automation (ICRA), 2016 IEEE International Conference on*, pages 1794–1801, 2016.

[19] S. Seok, A. Wang, M.Y. Chuah, D. Otten, J. Lang, and S. Kim. Design principles for highly efficient quadrupeds and implementation on the mit cheetah robot. In *2013 IEEE International Conference on Robotics and Automation (ICRA)*, pages 3307–3312. IEEE, 2013.

[20] K. Sreenath, HW Park, and J.W. Grizzle. Embedding active force control within the compliant hybrid zero dynamics to achieve stable, fast running on mabel. *IJRR*, 33:988–1005, Jun 2014.

[21] M. Srinivasan and A. Ruina. Computer optimization of a minimal biped model discovers walking and running. *Nature*, 439:72–75, 2006.

[22] X. Weitao, Y. Yesilevskiy, and C. David Remy. Selecting gaits for economical locomotion of legged robots. *IJRR*, 2015.

[23] E. R. Westervelt, J. W. Grizzle, and D. E. Koditschek. Hybrid zero dynamics of planar biped walkers. *Automatic Control, IEEE Transactions on*, 48(1):42–56, Jan 2003.

[24] S.J. Wickler, D.F. Hoyt, E.A. Cogger, and M.H. Hirschbein. Preferred speed and cost of transport: the effect of incline. *Journal of Experimental Biology*, 203:2195–2200, 2000.

[25] H. Zhao, J. Horn, J. Reher, V. Paredes, and A. D Ames. Multicontact locomotion on transfemoral prostheses via hybrid system models and optimization-based control. *IEEE Transactions on Automation Science and Engineering*, 13(2):502–513, 2016.
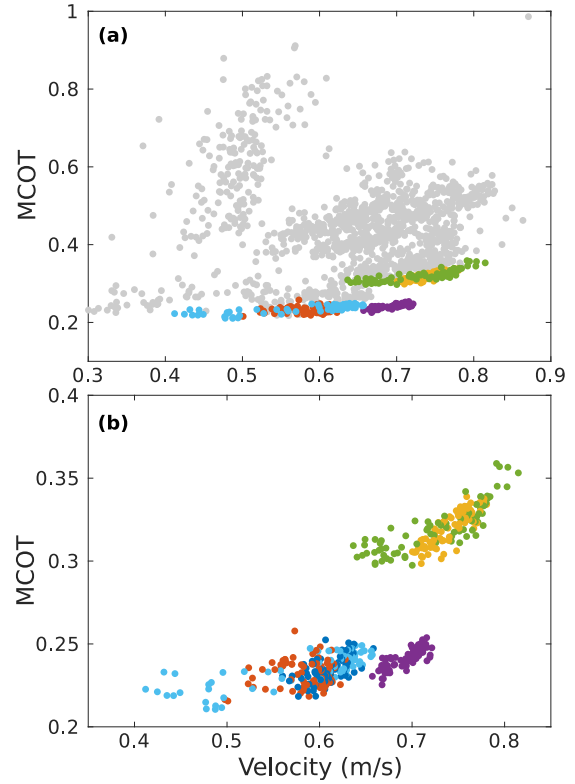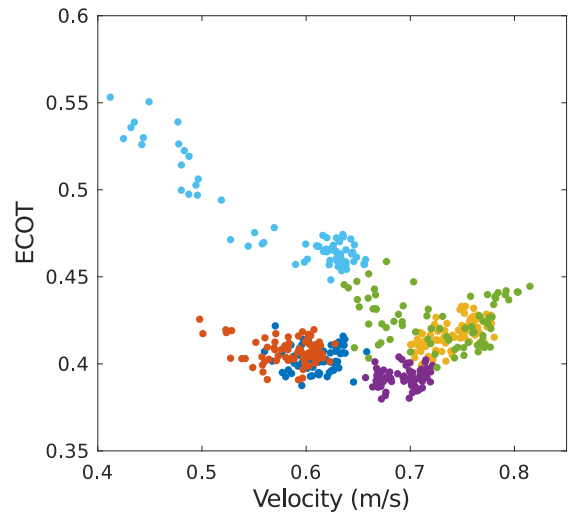
[26] H. Zhao, W.-L Ma, M. B. Zeagler, and A. D. Ames. Human-inspired multi-contact locomotion with amber2. In *Cyber-Physical Systems (ICCPS), International Conference on*, pages 199–210, April 2014.

[27] H. Zhao, J. Reher, J. Horn, V. Paredes, and A. D. Ames. Realization of nonlinear real-time optimization based controllers on self-contained transfemoral prosthesis. In *6th International Conference on Cyber Physics System*, pages 130–138, Seattle, WA, 2015.